# 5 GHZ LITHIUM NIOBATE MEMS RESONATORS WITH HIGH FOM OF 153

*Yansong Yang, Anming Gao, Ruochen Lu, and Songbin Gong*
University of Illinois at Urbana-Champaign, Urbana, IL, USA

## ABSTRACT

This paper reports on the demonstration of a new class of super-high frequency (SHF) microelectromechanical system (MEMS) resonators operating in the 5 GHz range. SHF resonances have been achieved using the first order antisymmetric (A1) mode, which features a phase velocity exceeding 10000 m/s in ion-sliced and suspended Z-cut Lithium Niobate ($LiNbO_3$) thin films. The fabricated device has demonstrated a high electromechanical coupling ($k_t^2$) of 29% and a high quality factor ($Q$) of 527 simultaneously. Consequently, this work marks the first time that MEMS resonators at SHF were demonstrated with an extremely high figure of merit (FoM= $k_t^2Q$) of 153. The SHF operation and high FoM of these A1 mode devices have showcased their potential as the key building blocks for future SHF front-end filters and multiplexers.

## INTRODUCTION

Recently, Internet of Things (IoT) has sparked interests in developing high performance wireless connectivity at super high frequencies (SHF) as the ultra-high frequencies (ULF) are already congested with broadcasting and communication applications. However, it remains a challenge to use SHF for IoT because wideband filters and multiplexers with a small form-factor are still largely unavailable for accessing the SHF without causing interferences to the neighboring bands.

One of the few promising technologies for implementing filters and multiplexers at SHF is microelectromechanical systems (MEMS) resonators. Their size scales with acoustic wavelengths, which are on the order microns at SHF. To achieve low insertion loss (*IL*), wide bandwidth (*BW*), and enhanced out of band rejection for the comprising filters, the MEMS resonators must feature a high figure of merit (FoM=$k_t^2 \cdot Q$). Previously, Aluminum Nitride (AlN) contour mode resonators (CMRs) have been investigated for SHF applications [1]. However, the FoM of AlN CMRs at SHF is limited (<5) with moderate electromechanical coupling ($k_t^2$ <2%). In addition, scaling CMRs toward SHF require ~100 nm wide electrodes, therefore requiring costly fine-resolution lithography and suggesting limited power handling. Other AlN devices, such as film bulk acoustic resonators (FBARs), can also operate at SHF [2]. Despite being sufficient to duplex WIFI bands around 5 GHz, they are limited in the factional bandwidth (FBW=3-6%) due to their moderate $k_t^2$ (6.5%). Thus, wider BW applications at SHF call for an even higher $k_t^2$ technology. Lithium Niobate ($LiNbO_3$) has recently emerged as an alternative thin film material for RF acoustics thanks to its pronounced piezoelectricity [3]. UHF Resonators of several lamb wave modes, including SH0 and S0, have been demonstrated in X-cut $LiNbO_3$ with $k_t^2$ > 20% and high $Q$ above 1000 simultaneously [4-9]. The higher $k_t^2$ promises a wider bandwidth for comprising filters while the high $Q$ enables lower insertion loss and sharper roll offs. Despite the demonstrated high FoMs of SH0 and S0 mode devices, their moderate phase velocities, 3500 m/s for SH0 and 6000 m/s for S0, make it difficult to scale towards SHF (>5 GHz). Thus, higher-order lamb wave modes with larger phase velocities are being investigated for demonstrating higher resonant frequency devices. In fact, 6.3 GHz $LiNbO_3$ devices using Chemical Vapor Deposition (CVD) and electrode reflectors have been demonstrated. However, only a moderate FoM was achieved due to the low quality of CVD thin films [10].

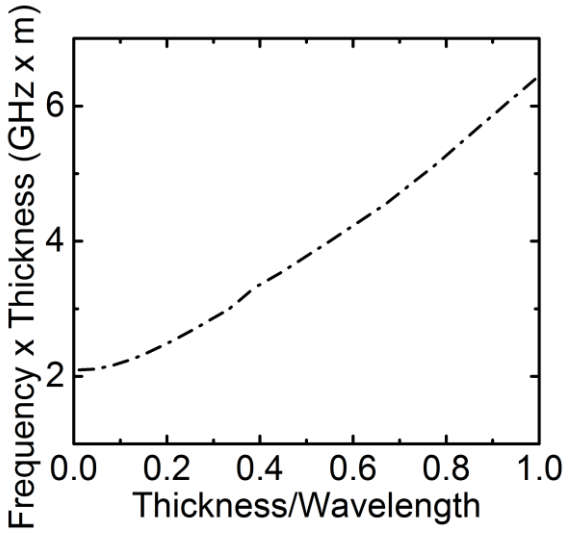

*Figure 1: Calculated dispersion curve for the A1 mode.*

In this study, we aim to realize SHF resonators based on the first-order antisymmetric (A1) Lamb-wave mode in ion-sliced Z-cut $LiNbO_3$ thin films. The ion-sliced $LiNbO_3$ thin films have single-crystal quality and permit a higher $Q$. The fabricated device with resonant frequencies around 5 GHz show very high $k_t^2$ and Q simultaneously, thus achieving a FoM of 153. In addition to the FoM, several key performance parameters, including temperature coefficient of frequency (TCF) and power handling, are also reported and discussed.

## DESIGN AND MODELING

Among various cuts of $LiNbO_3$, we select Z-cut as it has been theoretically shown to best support A1 mode excitation with high electromechanical coupling. In order to achieve an optimal device design, the characteristics of the A1 Lamb waves propagating in Z-cut $LiNbO_3$ films were first studied using COMSOL-based finite element analysis (FEA). Fig. 1 shows the calculated dispersion curve of the A1 mode as a function of the plate thickness ($h$) relative to wavelength ($\lambda$). The A1 mode has a high phase velocity and thus a resonant frequency over 5 GHz as the thickness of the $LiNbO_3$ plate is

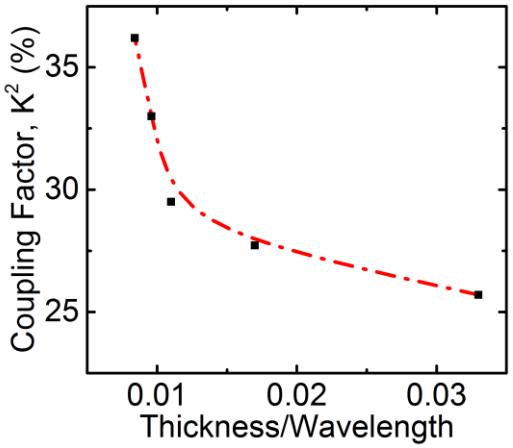


*Figure 2: Calculated coupling factor ($K^2$) of the A1 mode at various $h/\lambda$ values.*

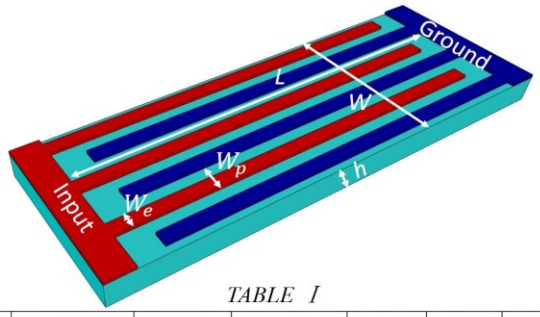


*TABLE I*

| Electrode Number ($N$) | Width of $LiNbO_3$ Plate ($W$) | Length of $LiNbO_3$ Plate ($L$) | Width of Electrode ($W_e$) | Width of Pitch ($W_p$) | Wave-length ($\lambda$) | Resonant Frequency ($f_c$) |
|---|---|---|---|---|---|---|
| 6 | 48 µm | 180 µm | 4 µm | 8 µm | 16 µm | 5.25 GHz |
| 2 | 38 µm | 120 µm | 6 µm | 19µm | 38 µm | 4.35 GHz |

*Figure 3: Typical MEMS resonator model. The design parameters of the resonators are listed in Table I.*

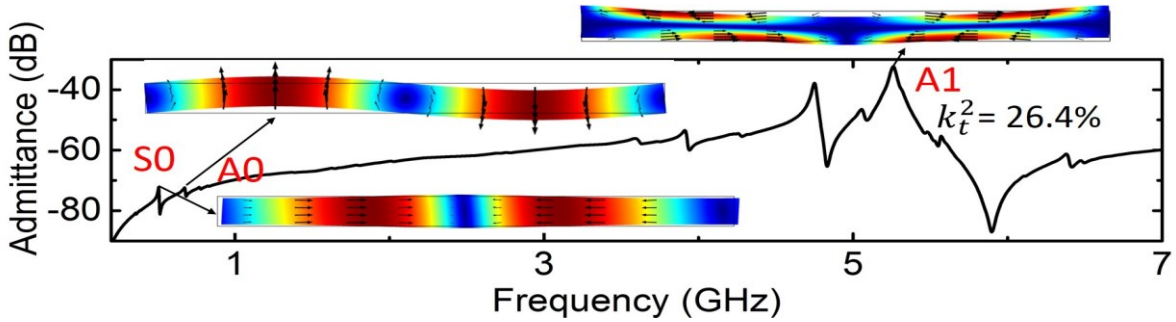


*Figure 4: Simulated response of a typical MEMS resonator based on Z-cut $LiNbO_3$ (400 nm). Displacement mode shapes of the S0, A0 and A1 modes are included (The arrows denote the displacement direction and amplitude).*

reduced to less than 400 nm. For a given thickness, Fig. 1 shows that the resonant frequency can be tuned by adjusting the electrode pitch width and hence the wavelength ($\lambda$).

The electromechanical coupling factor ($K^2$) of the A1 mode can be readily estimated by comparing the phase velocities of the same acoustic mode in a thin $LiNbO_3$ plate with and without perfect metallized boundary condition on the top surface [3]. Fig. 2 summarizes the calculated, $K^2$, for different $h/\lambda$ values smaller than 0.035. Note that the values of $K^2$ are all above 25%, and a smaller $h/\lambda$ results in a higher electromechanical coupling factor.

In addition to the analysis on wave characteristics, the SHF resonance and high electromechanical coupling ($k_t^2$) have also been confirmed by modeling a typical MEMS resonator. As seen in Fig. 3, the resonator in the model consists of a suspended Z-cut $LiNbO_3$ thin film with 6 pairs of interdigitated transducers (IDTs) on the top surface. The thickness of the Z-cut $LiNbO_3$ thin film is set to 400 nm, permitting a high phase velocity and a wide electrode pitch to attain a 5 GHz center frequency. The wide electrode pitch can be readily defined with standard photolithography tools (e.g mask aligners). The design parameters for the simulated resonator are listed in Table I.

The simulated response is shown in Fig. 4 with the displacement mode shapes of A1, A0 and S0 included in the insets. Similar to the analysis on wave characteristics, the simulation predicts a resonant frequency of 5.25 GHz for the A1

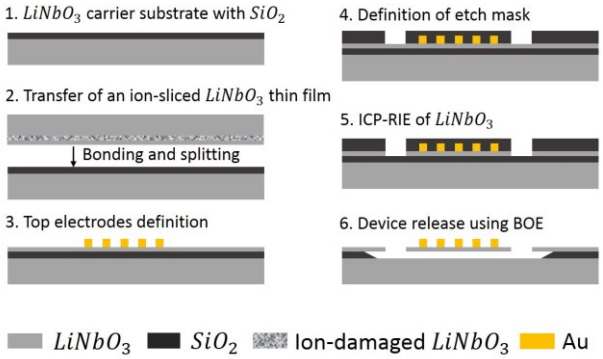


*Figure 5: Fabrication process for the $LiNbO_3$ resonators.*

mode, which are significantly higher than those of S0 and A0 modes. The device electromechanical coupling, $k_t^2$, is shown to be 26.4% and is on par with the calculated result in Fig. 2 for a Z-cut $LiNbO_3$ plate with $h/\lambda$=0.025.

Exploiting the dispersion shown in Fig. 1, the resonant frequency of A1 mode devices can also be tuned by setting the electrode pitch. The adjustment in electrode pitch affects the $h/\lambda$ for a given film thickness and hence modifies the acoustic velocity and resonant frequency. This feature permits the monolithic implementation of multi-frequency resonators and filters. To showcase this capability, a second device, with parameters also listed in Table I, was designed with

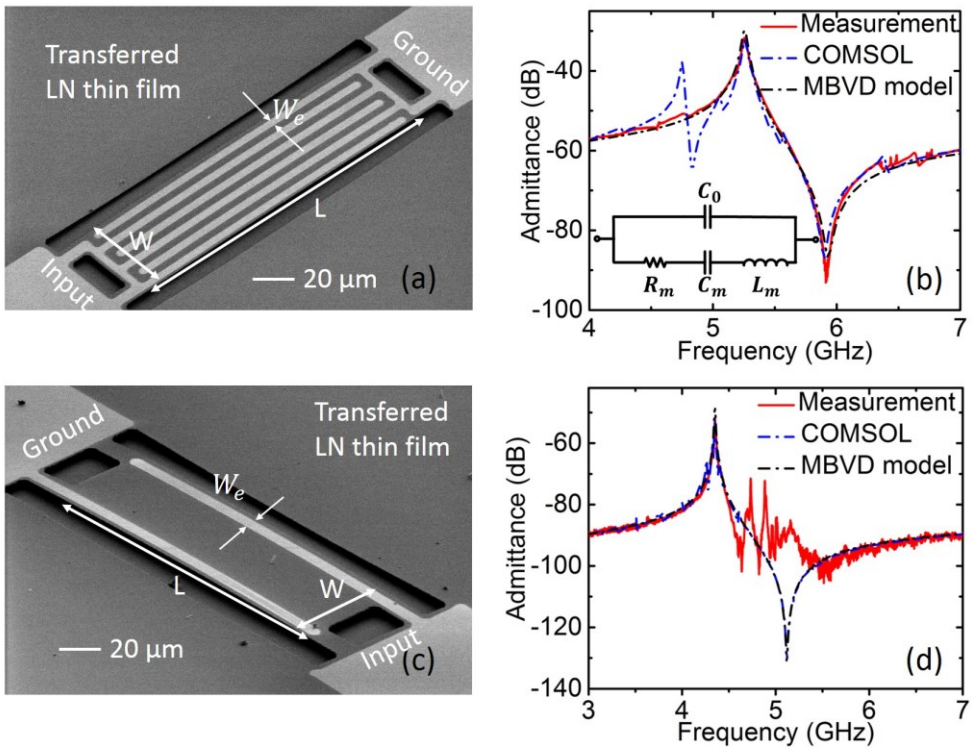


*TABLE II*

| Frequency | 5.25 GHz |
|---|---|
| Measured $Q$ | 112 |
| Extracted $k_t^2$ | 26.6% |
| Simulated $k_t^2$ | 26.4% |
| $C_0$ | 32 fF |
| $R_m$ | 31 Ω |
| $C_m$ | 8.7 fF |
| $L_m$ | 0.1 μH |

*TABLE III*

| Frequency | 4.35 GHz |
|---|---|
| Measured $Q$ | 527 |
| Extracted $k_t^2$ | 29% |
| Simulated $k_t^2$ | 30% |
| $C_0$ | 1.01 fF |
| $R_m$ | 236 Ω |
| $C_m$ | 0.39 fF |
| $L_m$ | 3.44 μH |

*Figure 6: (a) SEM image and (b) measured, COMSOL-modeled, and MBVD modeled response of the fabricated $LiNbO_3$ resonator with six electrodes. (c) SEM image and (d) measured, COMSOL-modeled, and MBVD modeled response of the fabricated $LiNbO_3$ resonator with two electrodes. Parameters of the MBVD model and key measured values are listed in Table II and III.*

two electrodes and a larger electrode pitch of 19 μm on the 400 nm Z-cut $LiNbO_3$ thin film. Note that, as seen in Fig. 2, changes in $h/\lambda$ also have effects on $K^2$. Nonetheless, for designs used here, high $K^2$ and large bandwidth can still be maintained. FEA confirms that the second design ($h/\lambda$=0.01) has an A1 resonance at 4.35 GHz with a simulated $k_t^2$ of 30%.

## FABRICATION AND RESULTS

To validate the simulation results, the A1 mode devices in Table I were fabricated with a process shown in Fig. 5. The fabrication starts from the ion slicing process in which a donor $LiNbO_3$ wafer is implanted with either H+ and He+ ions to induce micro-cracks at a few microns below the surface of the donor wafer. Post implantation, the donor wafer is subsequently bonded on a $LiNbO_3$ carrier substrate via a thin layer of $SiO_2$. Next, the thin film transfer process is carried out by subjecting the bonded wafer stack to a thermal process during which the donor wafer splits off at the layer where micro-cracks reside [11]. The $LiNbO_3$ thin film transfer process was done by NanoLN. Inc. For micromachining the devices, 50 nm-thick top electrodes (Au) are defined on top using a lift-off process. PECVD $SiO_2$ is subsequently deposited and later etched to serve as a hard mask for etching the $LiNbO_3$ resonator body. The patterning of the $SiO_2$ is done using $CHF_3$-based reactive ion etching (RIE) while the etching of $LiNbO_3$ thin film is done with $Cl_2$-based RIE and inductive coupled plasma (ICP). To suspend the resonator, the $SiO_2$ under and remaining $SiO_2$ hard mask on top of the $LiNbO_3$ thin film are removed at the same time with10:1 BOE-based wet etching. As the last step, critical point drying (CPD) is performed to dehydrate the resonators. The SEMs of the fabricated devices are shown in Fig. 6(a) and (c), respectively.

The fabricated devices were first characterized at room temperature and in dry air with an open chamber probe station and Keysight performance network analyzer. The measured admittance is shown in Fig. 6(b) and (d) respectively for the 6- and 2-electrode devices. The effects of the feedthrough capacitance ($C_f$) have been de-embedded using the measurement results of the on-chip test structures. As seen in Fig. 6(b), the 6-electrode resonator displays an A1 resonance at 5.25 GHz and an extracted $k_t^2$ of 26.6%, showing excellent agreement with the simulations. The modified Butterworth-Van Dyke (MBVD) model was used to extract the static capacitance $C_0$, $k_t^2$, and motional components ($R_m$, $C_m$, and $L_m$). The values of these parameters, along with the measured $Q$, are listed in Table II.

As seen in Fig. 6(c) and (d), in comparison to the 6-electrode device, the resonant frequency of the 2-electrode device is shifted to 4.35 GHz with an increased $k_t^2$ of 29%. The enhancement of $k_t^2$ is caused by a larger A1 mode wavelength and a smaller $h/\lambda$. These changes match the calculated characteristics of A1 shown in Fig. 1 and 2. The parameters of the

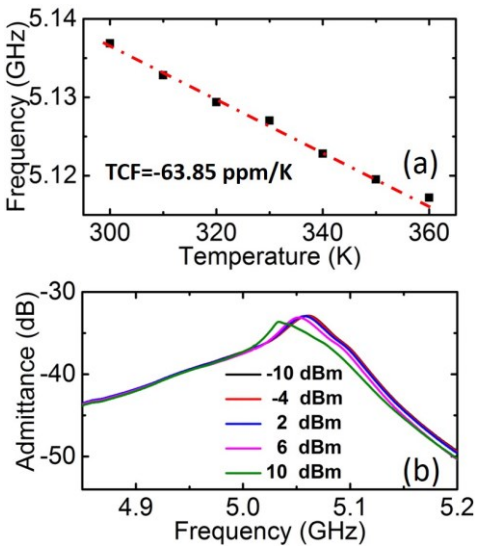


*Figure 7: (a) Measured TCF and (b) power handling of the A1 $LiNbO_3$ resonator with six electrodes.*

MBVD model and measured $Q$ are listed in Table III. Note that the measured $Q$ of 527 is much higher than that of the 6-electrode device. The reason for this $Q$ enhancement is still under investigation. As a result of the simultaneously measured high $k_t^2$ and $Q$, a record-high FoM of 153 has been demonstrated for MEMS resonators at SHF.

The TCF was also measured for the 6-electrode device. The measurements were performed in a Lakeshore cryogenic probe station. The measurements of the resonant frequency were cycled multiple times between 300 and 360 K in increments of 10 K. As seen in Fig. 7(a), the measured TCF is -63.85 ppm/K.

We also experimentally investigated the power-handling capability by measuring the device response at various input power levels. The input power was swept from -10 to +10 dBm for the A1 mode device with 6 electrodes. The results are shown in Fig. 7(b). The bifurcation, defined as the verge of instability, occurs beyond +10 dBm for the A1 mode device with 6 electrodes.

## CONCLUSION

In this work, A1 mode $LiNbO_3$ MEMS resonators with resonant frequencies in the 5 GHz range and FoM as high as 153 have been demonstrated. The super-high operating frequency and the high FoM were achieved by micromachining 400 nm ion-sliced Z-cut $LiNbO_3$ thin films to form the A1 mode resonators. The high FoM of 153 results from the simultaneously attained high $k_t^2$ of 29% and Q of 527. The capability of lithographically setting the resonant frequency of A1 mode devices has also been studied and confirmed by simulating and testing devices with different electrode pitches and $h/\lambda$ (0.01 and 0.025). Detailed characterizations on device $Q$, static capacitance $C_0$, TCF, and power handling are also presented and analyzed.

## REFERENCE


[1] M. Rinaldi, C. Zuniga, C. Zuo, and G. Piazza, "Super-high-frequency two port AlN contour-mode resonators for RF applications," *IEEE Trans. Ultrason. Ferroelectr. Freq. Control*, vol. 57, pp. 38-45, Jan. 2010.

[2] Satoh, Yoshio, Tokihiro Nishihara, Tsuyoshi Yokoyama, Masafumi Iwaki, and Tsutom Miyashita. "Development of 5GHz FBAR filters for wireless systems." *In Sec. Int. Symp. on Acoust. Wave Dev. for Fut. Mob. Commun. Syst*. 2004.

[3] S. Gong and G. Piazza, "Design and Analysis of Lithium-Niobate-Based High Electromechanical Coupling RF-MEMS Resonators for Wideband Filtering," *IEEE Trans. on Microw. Theory and Techn.*, Vol. 61, no. 1, pp. 403-414, Jan. 2013.

[4] S. Gong and G. Piazza, "Figure-of-merit enhancement for laterally vibrating lithium niobate MEMS resonators," *IEEE Trans. Electron Devices*, vol. 60, no. 11, pp. 3888-3894, Nov 2013.

[5] R. H. Olsson III, K. Hattar, M. S. Baker, M. Wiwi, J. Nguyen, C. Padilla, S. J. Homeijer, J. R. Wendt, and T. A. Friedmann, "Lamb wave micromechanical resonators formed in thin plates of lithium niobate," *Hilton Head Solid-State Sensors, Actuators and Microsystems Workshop*, 2014, pp. 281–284.

[6] R. H. Olsson III, K. Hattar, S. J. Homeijer, M. Wiwi, M. Eichenfield, D. W. Branch, M. S. Baker, J. Nguyen, B. Clark, T. Bauer, T. A. Friedmann, "A high electromechanical coupling coefficient SH0 Lamb wave lithium niobate micromechanical resonator and a method for fabrication," *Sensors and Actuators A: Physical*, Volume 209, 1 March 2014, Pages 183-190.

[7] Y. H. Song and S. Gong, "Elimination of Spurious Modes in SH0 Lithium Niobate Laterally Vibrating Resonators," *IEEE Electron Device Letters*, vol. 36, no. 11, pp. 1198-1201, Nov. 2015.

[8] R. Wang, S. A. Bhave, S. Zhgoon, and K. Bhattacharjee. "Multi-frequency LiNbO3 Lamb wave resonators with<3Ω impedance." *2016 IEEE 29th International Conference on Micro Electro Mechanical Systems (MEMS)*, pp. 679-682. IEEE, 2016.

[9] S. Gong and G. Piazza, "Monolithic Multi-Frequency Wideband RF Filters Using Two-Port Laterally Vibrating Lithium Niobate MEMS Resonators," *Journal of Microelectromechanical Systems*, vol. 23, no. 5, pp. 1188-1197, Oct. 2014.

[10] M. Kadota, T. Ogami, K. Yamanoto, H. Tochishita and Y. Negora, "High-Frequency Lamb Wave Device Composed of MEMS Structure Using LiNbO3 Thin Film and Air Gap," *IEEE Trans. Ultrason. Ferroelectr. Freq. Control*, vol. 57, no. 11, NOV 2010.

[11] H. Hu, F. Lu, F. Chen, B-R. Shi, K-M. Wang, and D-Y. Shen. "Monomode optical waveguide in lithium niobate formed by MeV Si+ ion implantation." *Journal of applied physics* 89 (2001): 5224-5226.


# CONTACT


*Y. Yang, yyang165@illinois.edu
S. Gong, songbin@illinois.edu